Journal of Structural Geology, Vol. 2, No. 1/2, pp. 119 to 126.
Pergamon Press Ltd. 1980. Printed in Great Britain.

0191-8141/80/0601-0019 $02.00/0

Development of sheath folds in shear regimes

P. R. COBBOLD and H. QUINQUIS

Centre Armoricain d'Etude Structurale des Socles
(CNRS—Université de Rennes), Campus de Beaulieu, 35042 Rennes-Cedex, France

(Received 17 May 1979; accepted in revised form 19 July 1979)

Abstract—The development of three-dimensional fold shapes in shear regimes is studied using theoretical and experimental methods and with reference to natural examples. Theoretical studies are based on homogeneous simple shear and other valid solutions to the equations of motion of Newtonian materials. Experimental work has been done with models made from analogue materials and deformed in a simple shear machine capable of large shear strains ($\gamma > 10$). Emphasis is placed on passive folds. Three models are presented for their development, two models invoking flow with steady stream lines, the third involving unsteadiness accompanying boudinage. Resulting sheath folds are strongly asymmetric, with curved fold hinges. Geological examples of sheath folds occur in many natural shear zones and may have formed in an essentially passive manner.

INTRODUCTION

IN THIS paper we consider the development of three-dimensional fold shapes in systems where the bulk deformation is a progressive simple shear. As a first approximation, our results are therefore applicable to geological situations such as shear zones, the bases of nappes, and diapir margins, where deformation is perhaps complex but where the major component is a simple shear. Studies of such zones have shown that internal folds are often strongly non-cylindrical or even sheathlike in appearance (Dalziel & Bailey 1968, Carreras *et al.* 1977, Rhodes & Gayer 1977, Quinquis *et al.* 1978). Fold axes are curved within the axial planes. A statistical analysis of fold axial directions shows a strong frequency maximum centred about the maximum principal axis of the bulk strain ellipsoid. This has been interpreted in terms of progressive rotation of linear elements towards the extension direction (Borradaile 1972, Sanderson 1973, Escher & Watterson 1974, Bell 1978). The interpretation is justified for homogeneous deformation of passive folds (Donath & Parker 1964) where the folded layering is rheologically no different from its surroundings. For active folds, where the layering has distinct rheological properties, deformation may be locally heterogeneous and unstable. The passive model may then be a poor, if useful, first approximation to what really occurs.

The development of passive folds at the bases of ice sheets and nappes has been modelled numerically by Hudleston (1976, 1977), but in two dimensions. Active folds in shear regimes have been modelled experimentally (e.g. Ramberg 1959, Ghosh 1966, Manz & Wickham 1978, Ramberg & Johnson 1976, Reches & Johnson 1976) and theoretically (Treagus 1973, Ramberg & Johnson 1976, Reches & Johnson 1976), but only for small shear strains (up to $\gamma = 2$) and only in two dimensions. Here we wish to consider large shear strains ($\gamma > 10$) and three-dimensional fold shapes. We deal with passive folds because (a) they are easier to model, and (b) a preliminary appreciation of the essentially kinematic processes of passive folding is necessary before a confident study of active folds is undertaken.

Hudleston (1976, 1977) has shown clearly that a necessary condition for passive folds to develop is that the layering be oblique to the stream lines in the material. Such an obliquity may be present at the onset of deformation or it may appear if the stream lines are unsteady in orientation. If the stream lines become or remain steady (this is motion with steady stream lines, Truesdell & Toupin 1960, p. 431), the obliquity diminishes progressively as the layering rotates towards the stream lines. Any early folds become isoclinal and no new fold can develop, unless of course the stream lines lose their steadiness. In Hudleston's models, unsteadiness results from a change in boundary conditions (an increase in ice thickness). Here we will consider unsteadiness linked to internal instability of the system.

Three models are presented for the development of passive folds (Fig. 1). The first two invoke steady stream lines, whereas the third involves unsteadiness accompanying boudinage. The models are studied theoretically and experimentally. Theoretical studies are based on homogeneous simple shear and other valid solutions to the equations of motion of Newtonian materials.

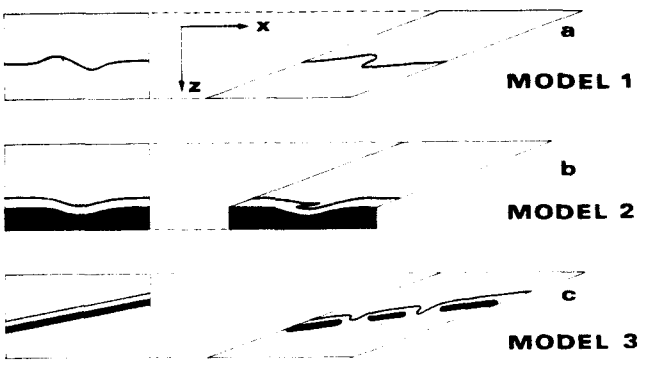

Fig. 1. Three models of passive fold formation in bulk simple shear. In Model 1, deformation is homogeneous. In Model 2, deformation is perturbed by a resistant layer (solid black area) with initial deflection. In Model 3, deformation is perturbed by a boudinaging layer oblique to the shear direction.

Experimental work has been done with models made from analogue materials deformed in a simple shear machine capable of large shear strains.

PASSIVE FOLDING IN MOTION WITH STEADY STREAM LINES

We consider two models in which the stream lines are steady. Folds develop by passive amplification of initial deflections in an otherwise planar and passive layering which is grossly parallel to the shearing plane (Fig. 1). Geologically this situation might occur for example at the base of a nappe, the layering being bedding. Such a layering is rarely if ever perfectly planar: instead local deflections are common as a result, for example, of initial thickness variations, lateral facies changes, channel infills and so on. Moreover, natural deflections of this kind are generally non-cylindrical. Many are also symmetrical about the bedding normal.

Model 1

We assume homogeneous simple shear with the shearing plane parallel to the sheet dip of the layering (Fig. 2). As a result of deformation, any initially symmetrical deflections become strongly asymmetric, with one limb longer than the other. The sense of asymmetry (clockwise in Fig. 2) is a result of the dextral sense of shear. The hinge line itself becomes more strongly curved and the fold therefore more non-cylindrical. The final fold shape depends upon the shape of the initial deflection and on the total shear strain; it is independent by definition of the deformation history. At high shear strains ($\gamma > 10$), most deflections of realistic geological proportions become sheathlike. Notice that in simple shear the amplitude (measured along z) and the hinge span (measured along y) remain constant by definition. As a result a cross-section normal to x reveals a closed elliptical trace, with short axis parallel to z. Shapes of this kind occur and have been described (eyes) in rocks from natural shear zones (Fig. 3). It is possible that many such natural shapes have been formed almost passively during nearly homogeneous deformation.

The development of passive sheath folds in homogeneous deformation has also been followed experimentally using silicone models (see Appendix 1 for details of experimental procedure). In one experiment, a multilayered model was constructed with passive layering (Fig. 4). Initial deflections were introduced during construction. After deformation in the simple shear machine, the initial deflections became sheath folds (Figs. 4 and 5). Other non-cylindrical folds appeared unexpectedly in the model and can be attributed to (a) imperfections in model construction, (b) boundary effects due to friction, and (c) air bubbles at layer surfaces. In our experience with models of this kind, the formation of sheath folds is hard to avoid.

Model 2

We consider a bulk simple shearing, perturbed by the presence of resistant layers grossly parallel to the shearing plane but with surface asperities (Fig. 1b). This model generalizes the preceding one to systems with rheological layering. Again a geological application of the model is the base of a nappe.

If the resistant layers are completely rigid, the motion elsewhere will have steady stream lines. This has been modelled theoretically for the special case of a single rigid layer sandwiched between two infinite half-spaces of Newtonian material with uniform viscosity. Using methods of conformal representation (Appendix 2), an exact two-dimensional solution has been obtained for the velocities about a rigid layer with periodically spaced asperities of finite amplitude (Fig. 6). Next to the layer, the stream lines are parallel to the interface but the amplitude of this disturbance decays with distance from the layer (cf. Hudleston 1976, fig. 9). Any line in the matrix not parallel to a stream line will deform; some will develop folds. For example, consider a line (L–L', Fig. 6) which is the locus of points at a constant orthogonal

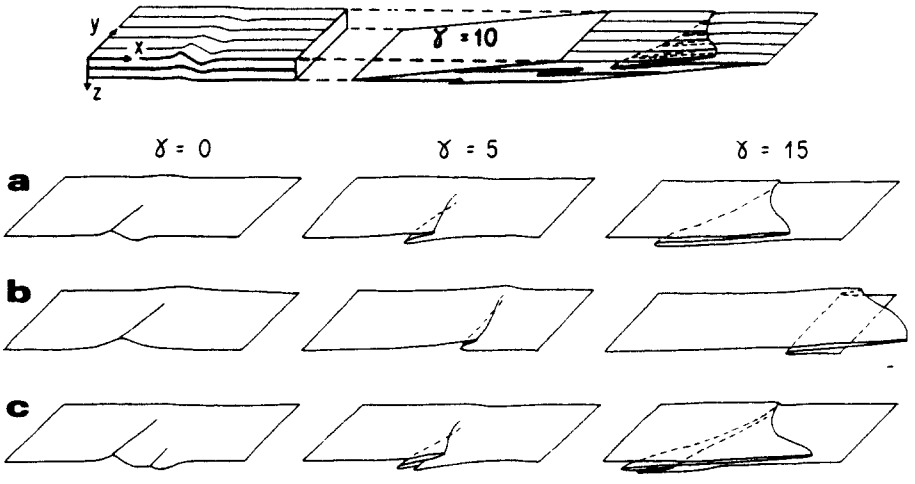

Fig. 2. Model 1: theoretical results. Noncylindrical initial deflections of various shapes (a, b & c) have been deformed in simple shear (top: x = shear direction, xy = shearing plane). Folds become asymmetric at moderate shear strains ($\gamma = 5$) and strongly noncylindrical at high shear strains ($\gamma = 15$).

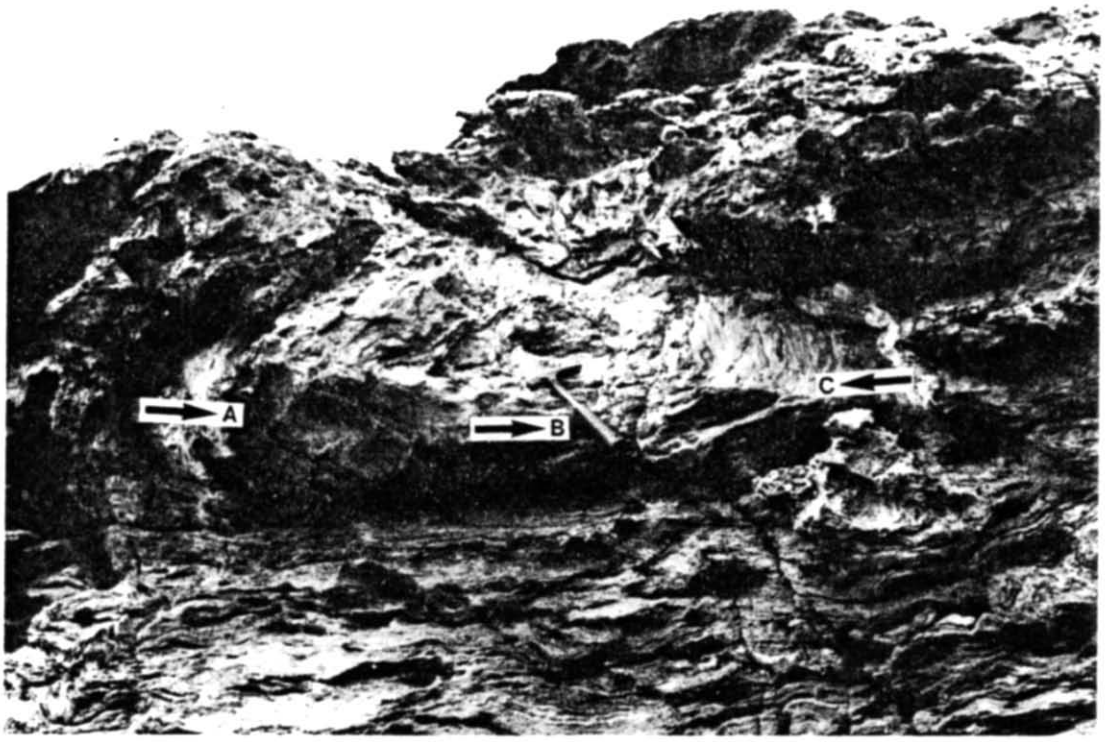

(a)

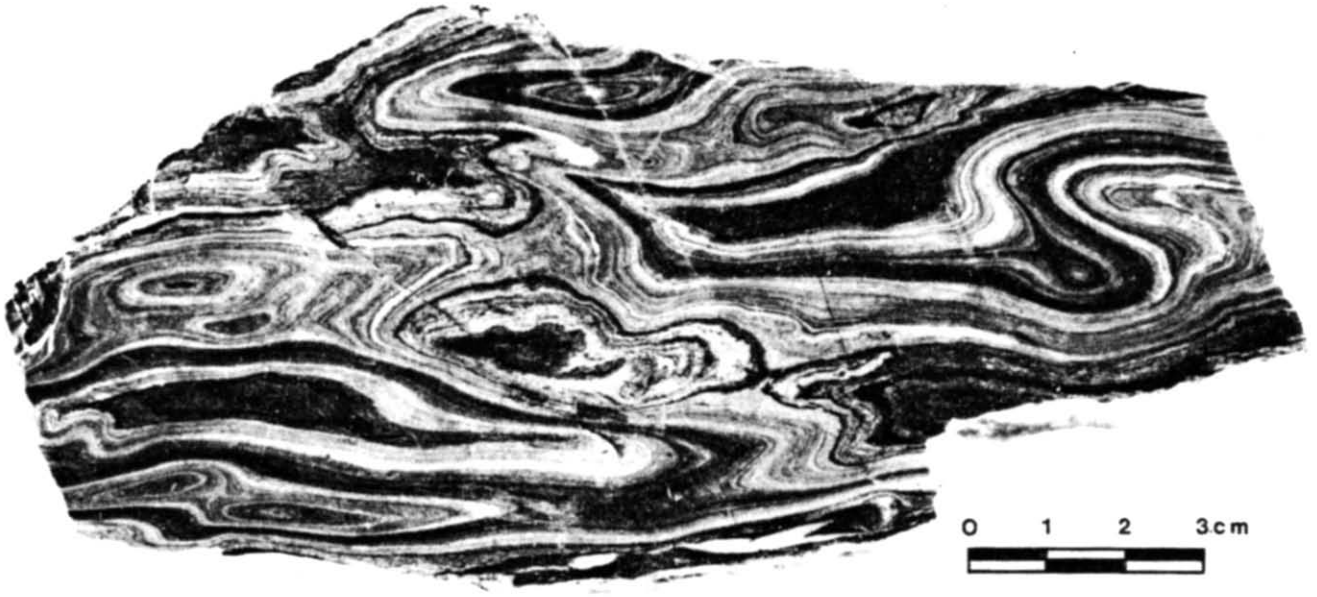

(b)

Fig. 3. Natural examples of sheath folds. (a) Nose region of sheath exposed in vertical E–W sea-cliff at Vallon du Lavoir, Quehello, Ile de Groix, France (47°30′N, 5°50′ W). Arrows indicate declination of fold hinge (110° at A, 060° at B, 200° at C). (b) Section normal to long axes of sheaths in mylonitic rocks from Vang, Valdres, Norway (specimen courtesy of A. G. Milnes). Notice elliptical eyelike traces.

Fig. 5. Photograph of serial section 11, Model 1 (for location, see Fig. 4). Model is built of passive silicone layers of alternating colour. Central layer (black) is that of Fig. 4. Eyelike traces are cross-sections of sheaths.

Fig. 9. Photograph of serial section No. 9, Model 3 (for location, see block diagram of Fig. 8).

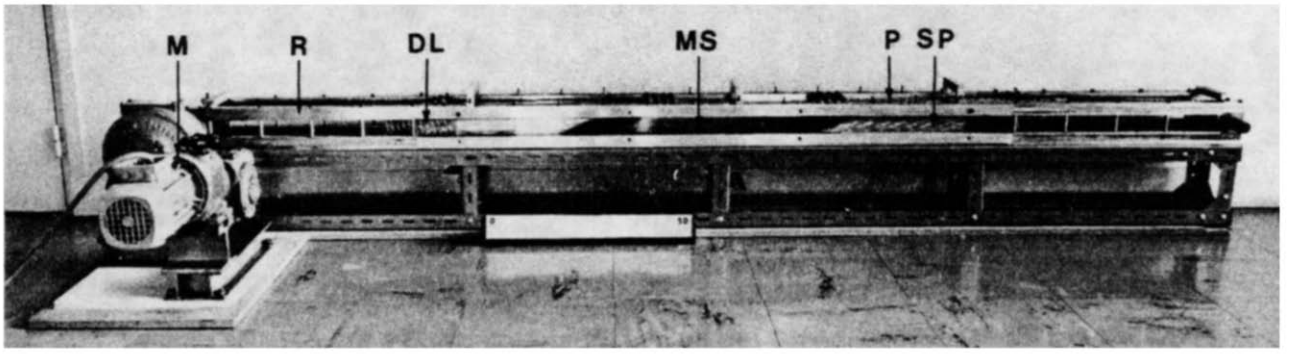

Fig. 10. Simple shear machine. The central space (MS) will house a model. Shear stress is applied to the upper and lower surfaces of the model through stiff plates (P) which slide along rails (R) under the action of a chain and sprockets driven by a motor (M). Lateral confinement is provided by stationary Perspex walls (transparent). The ends of the model are supported by a stack of sliding plates (SP), each one positioned by an accordion-like distance linearizer (DL). The model space as illustrated has a dextral shear strain of $\gamma = 1.5$. The rectangular white scale bar is 50 cm long.

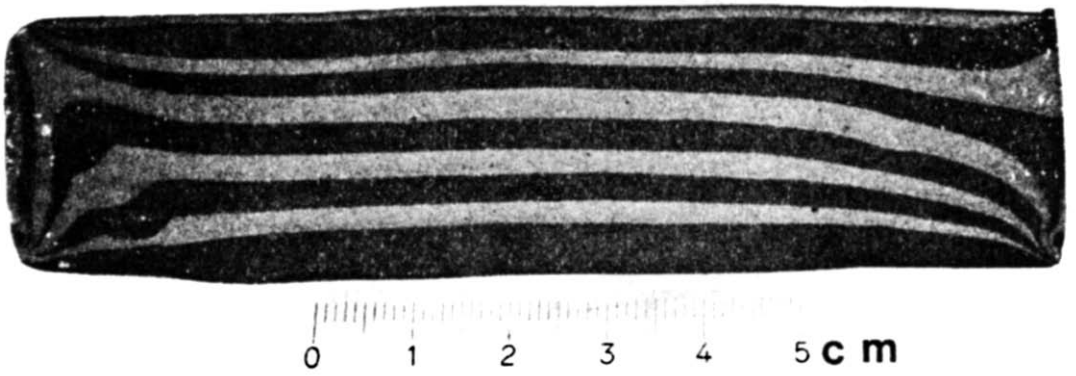

Fig. 11. Homogeneity of deformation ($\gamma = 16$). This section through a silicone model is normal to the shear direction. The layers are of contrasting colour but the same rheology. Before deformation each layer was approximately planar, of even thickness and normal to the shear direction. Folds and thickness variations now visible result mainly from adherence of the model boundaries (left and right) to the stationary confining walls of the simple shear machine. Notice that boundary disturbances diminish rapidly towards the centre of the model.

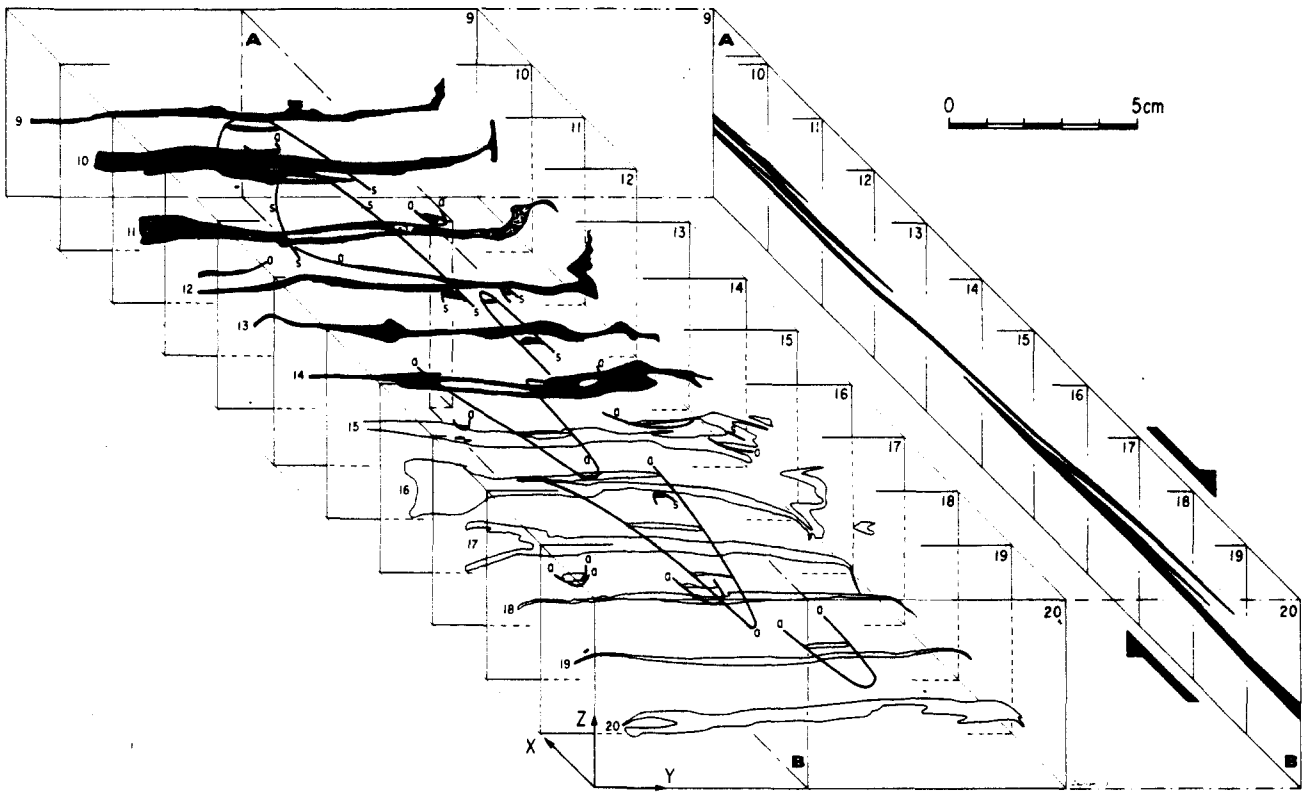

Fig. 4. Model 1: experimental result ($\gamma = 10$). Serial sections (numbered 9–20) through a layered silicone model are shown in isometric projection (block diagram). They are normal to the shear direction (x). Arrows show sense of shear. Only the central layer of the model is shown. Hinge-lines of antiforms (a) and synforms (b) have been interpolated. A longitudinal section (AB, right) shows strong asymmetry of folds. Other layers are illustrated in Fig. 5.

distance from the rigid boundary. Using the exact solution for the velocities (Appendix 2), the new position of each point has been calculated for a time interval equivalent to a bulk shear strain of $\gamma = 10$. The new locus (M–M') has a strongly asymmetric, nearly isoclinal fold. The result is similar to that obtained by Hudleston (1976) using a numerical model based on non-Newtonian behaviour.

A similar but three-dimensional model has been investigated experimentally using a matrix of silicone putty and a single resistant embedded layer of plasticine. Before assembly with the matrix, the surface of the plasticine layer was indented so as to create an initial non-cylindrical deflection. The matrix was then added in layers of contrasting colours but of constant thickness and rheology. The model was deformed in the simple shear machine and serially sectioned. The resulting reconstruction (Fig. 7) reveals a passive non-cylindrical fold whose profile (along the plane of mirror symmetry normal to y) is very similar to that obtained in the two-dimensional theoretical model (Fig. 6).

PASSIVE FOLDING IN MOTION WITH UNSTEADY STREAM LINES

Model 3

Here we suppose that during bulk simple shearing an unsteadiness of stream lines is caused by the onset and progressive development of boudinage in relatively resistant layers (Fig. 1c). The layering is oblique to the bulk shear direction and the angle between them diminishes progressively. This is the situation envisaged by Hudleston (1976) for steady stream lines, but here it is generalised to include relatively resistant layers which boudinage and cause unsteadiness. Geologically this situation is to be expected in shear zones of all kinds. The model is especially applicable to layered metamorphic rocks.

We have investigated this model experimentally. A single resistant layer (75% by weight plasticine, 25% silicone putty) was embedded in a matrix of silicone putty with colour banding. The layering was made as planar as possible with no deliberate initial deflections. It was placed in the simple shear machine at an initial angle of 10° to the shear direction and deformed to a shear strain of $\gamma = 12.5$. During the experiment, the resistant layer was observed to boudinage progressively. Early necking and rupture occurred at selected sites. The boudins so formed then separated, matrix material filling the intervening gaps. Further ductile extension within the boudin segments led to renewed necking and rupture, with a consequent increase in the total number of boudins. A reconstruction of the deformed model (Fig. 8) shows that boudin axes are not all normal to the shear direction. The boudins themselves are non-cylindrical and some axes intersect cross sections drawn normal to y. This could give the false impression that bulk extension occurred along y. The origin of the oblique axes is attributable to: (a) rotation of line elements towards the extension direction, (b) formation of

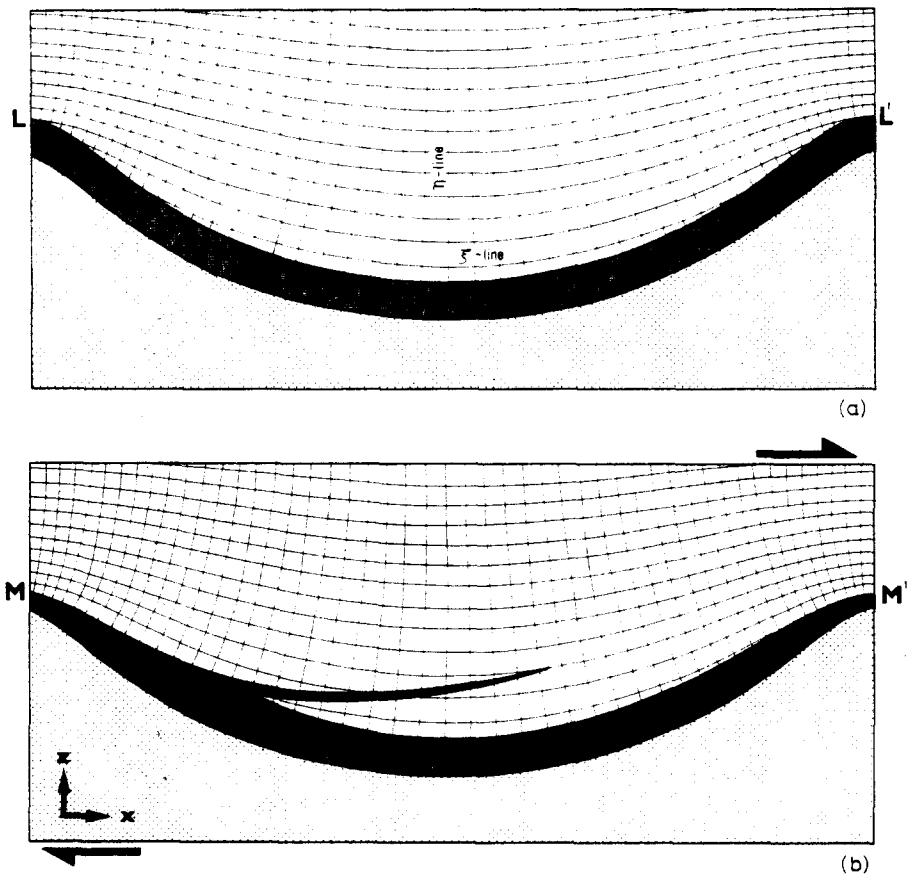

Fig. 6. Model 2: theoretical solution ($\gamma = 10$). A rigid layer (stippled), with periodically spaced asperities of finite amplitude, is overlain by a Newtonian matrix with a passive layer at the base (dark). In the undeformed state (a), the passive layer is of constant thickness. Under the action of a dextral shear stress (arrows), the matrix flows. The flow velocity at each point is derived in Appendix 2. Curved orthogonal gridlines in the matrix are curvilinear coordinates. Those trending from left to right (ξ-lines) are also stream lines and particle path-lines. After deformation (b), the passive layer is strongly folded.

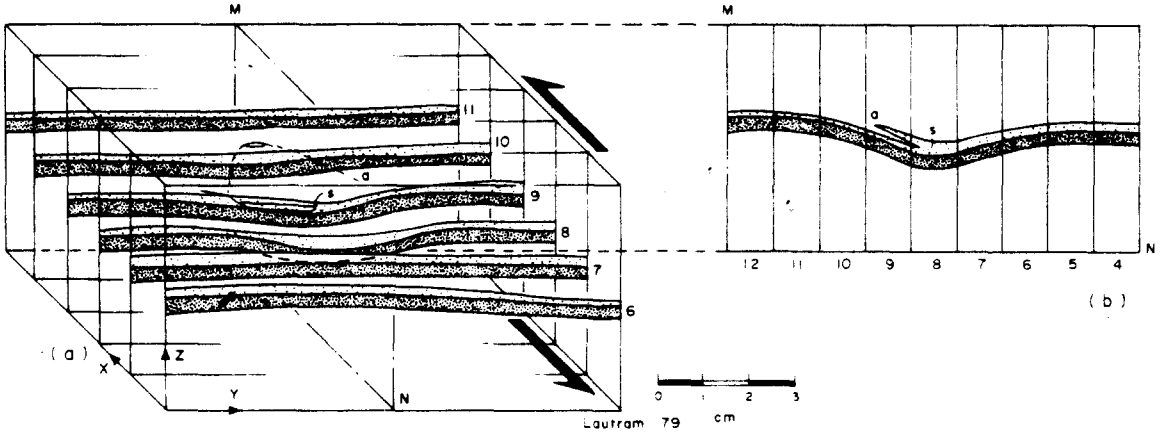

Fig. 7. Model 2: experimental result ($\gamma = 14$). Serial sections (6–11) through a layered model are shown in isometric projection (a). The shear direction and shear sense are shown by arrows. A single resistant layer (darker shade) is of plasticine. The other layer shown (lighter shade) is of silicone. The rest of the model is also of silicone. Hinge lines of an antiform (a) and synform (s) have been interpolated. Both folds are derived from an initial deflection. Their asymmetry is apparent in the longitudinal section (b).

Fig. 8. Model 3: experimental result ($\gamma = 12.5$). Serial sections (1–11) through a layered model are shown in isometric projection. Arrows show the shear direction and shear sense. Steplike boundaries of the model were caused by the boundary plates of the simple shear machine (see Appendix 1). Widely separated boudins of a plasticine/silicone mixture (black elliptical shapes) are surrounded by passive layers of silicone (wavy black lines and folds). All are set in a silicone matrix (not illustrated here—see Fig. 9).

axes in an oblique position by shear failure of the resistant layer, or (c) a combination of both.

Non-cylindrical passive folds are visible in the colour-banded matrix (Fig. 9). These are developed mainly in the regions between separated boudins and we interpret them as follows. Inflow of matrix into boudin necks produces deflections in the passive layering. Stream lines in the matrix are not parallel to the layering, which therefore becomes deformed and locally folded in the manner of Model 2. As the boudin segments separate, the folds remain in the region between them. Because the boudins are non-cylindrical, so are the folds. The non-cylindricity of the passive folds increases with progressive deformation. Notice that other folds have formed near the model boundaries, probably as a result of step-like indentation by the boundary plates of the machine (see Appendix 1 for details).

Model 3 has many geological implications. It shows how unsteadiness in flow can arise naturally as a result of internal mechanical instability. Generation of new folds can be expected each time instability is reactivated (e.g. by formation of boudins). Associations of boudinage and non-cylindrical folds occur in natural examples, such as the Ile de Groix blueschists (Quinquis *et al.* 1978). A boudinaging layer can be effectively a fold source, active throughout the entire history of deformation.

CONCLUSIONS

1. In systems undergoing bulk simple shearing, passive folds can develop by kinematic amplification of deflections. These may be present before deformation, or they may form as a result of internal mechanical instability.

2. Such passive folds are strongly asymmetric and in most cases non-cylindrical, if not sheathlike.

3. Many natural sheath folds may have developed in an essentially passive manner.

4. Three models for passive fold development in shear regimes have been investigated theoretically or experimentally. The models are simple yet applicable to fold formation in nappes and shear zones in general. More complex models may be more realistic, but are expected to give essentially the same results.

5. If passive folds are formed by homogeneous deformation, they are in consequence independent of the deformation path and can only be correlated with the finite strain ellipsoid. Passive folds with truly sheathlike forms are therefore not diagnostic of shear regimes: nevertheless they may be key factors in helping identify such regimes, especially when considered together with all the other structural evidence (see Quinquis *et al.* 1978).

6. Three-dimensional shapes of active folds in shear regimes have not yet been investigated. By analogy with results for coaxial regimes (e.g. Dubey & Cobbold 1977) active folds in shear regimes are likely to be more cylindrical than their passive counterparts.

7. Folds may be generated episodically throughout an entire history of progressive shearing, as a result of episodic instability of the flow. Successive refolding of metamorphic fabrics is also likely (see Quinquis *et al.* 1978).

REFERENCES

Bell, T. H. 1978. Progressive deformation and reorientation of fold axes in a ductile mylonite zone: the Woodroffe Thrust. *Tectonophysics* **44**, 285–320.

Borg, S. 1963. *Matrix-tensor Methods in Continuum Mechanics*. Van Nostrand, New York.

Borradaile, G. J. 1972. Variably oriented co-planar primary folds. *Geol. Mag.* **109**, 89–98.

Carreras, J., Estrada, A. & White, S. 1977. The effects of folding on the C-axis fabrics of a quartz mylonite. *Tectonophysics* **39**, 3–24.

Dalziel, I. W. D. & Bailey, S. W. 1968. Deformed garnets in a mylonitic rock from the Grenville Front and their tectonic significance. *Am. J. Sci.* **266**, 542–562.

Donath, F. A. & Parker, R. B. 1964. Folds and folding. *Bull. geol. Soc. Am.* **75**, 45–62.

Dubey, A. K. & Cobbold, P. R. 1977. Noncylindrical flexural slip folds in nature and experiment. *Tectonophysics* **38**, 223–239.

Escher, A. & Watterson, J. 1974. Stretching fabrics, folds and crustal shortening. *Tectonophysics* **22**, 223–231.

Ghosh, S. K. 1966. Experimental tests of buckling folds in relation to strain ellipsoid in simple shear deformations. *Tectonophysics* **3**, 169–185.

Hudleston, P. J. 1976. Recumbent folding in the base of the Barnes Ice Cap, Baffin Island, Northwest Territories, Canada. *Bull. geol. Soc. Am.* **87**, 1684–1692.

Hudleston, P. J. 1977. Similar folds, recumbent folds, and gravity tectonics in ice and rocks. *J. Geol.* **85**, 113–122.

Jaeger, J. C. 1969. *Elasticity, Fracture and Flow*. Methuen, London.

Jaeger, J. C. & Cook, N. G. W. 1971. *Fundamentals of Rock Mechanics*. Chapman & Hall, London.

McClay, K. R. 1976. The rheology of plasticine. *Tectonophysics* **33**, T7–T15.

Manz, R. & Wickham, J. 1978. Experimental analysis of folding in simple shear. *Tectonophysics* **44**, 79–90.

Mushkelishvili, N. I. 1953. *Some Basic Problems of the Mathematical Theory of Elasticity*, 4th edition, (translated by Radok, J. R. M.) P. Noordhoff, Groningen.

Quinquis, H., Audren, C., Brun, J. P. & Cobbold, P. R. 1978. Intense progressive shear in Ile de Groix blueschists and compatibility with subduction or obduction. *Nature, Lond.* **273**, 43–45.

Ramberg, H. 1959. Evolution of ptygmatic folding. *Norsk geol. Tidsskr.* **39**, 99–152.

Ramberg, I. B. & Johnson, A. M. 1976. A theory of concentric, kink and sinusoidal folding and of monoclinal flexuring of compressible elastic multilayers. Part V. Asymmetric folding in interbedded chert and shale of the Franciscan Complex, San Francisco Bay area, California. *Tectonophysics* **32**, 295–320.

Reches, Z. & Johnson, A. M. 1976. A theory of concentric, kink and sinusoidal folding and of monoclinal flexuring of compressible elastic multilayers. Part VI. Asymmetric folding and monoclinal kinking. *Tectonophysics* **35**, 295–334.

Rhodes, S. & Gayer, R. A. 1977. Non-cylindrical folds, linear structures in the X direction and mylonite developed during translation of the Caledonian Kalak Nappe Complex of Finmark. *Geol. Mag.* **114**, 329–341.

Sanderson, D. J. 1973. The development of fold axes oblique to the regional trend. *Tectonophysics* **16**, 55–70.

Treagus, S. H. 1973. Buckling stability of a viscous-layer system oblique to the principal compression. *Tectonophysics* **19**, 271–289.

Truesdell, G. & Toupin, R. 1960. The classical field theories. *Handb. Phys.* **3**, 226–793.

APPENDIX 1

EXPERIMENTAL PROCEDURE

Model materials

Only two materials were used, silicone putty (Rhodorsil[R] Gomme

Speciale GS1R, manufactured by Rhone-Poulenc, France) and plasticine (Standard Violet Plasticine, manufactured by Harbutt's Ltd., England). According to the manufacturers' data, the silicone putty has an almost perfectly linear dependence of stress upon strain-rate, for temperatures ranging from − 40°C to + 100°C and shear stresses less than 100 bars (10 MPa). The viscosity ranges from 10^7 poise (10^6 Pa s) at − 40°C through 1.6×10^5 poise at + 20°C to 10^3 poise at + 100°C. As manufactured the silicone is pale rose in colour. Batches of various darker tones were prepared by admixing small amounts of finely powdered iron oxide (Fe_2O_3). This mineral pigment and the silicone are chemically inert and the mixture is stable. Small differences in viscosity were detected between the mixture and the pure silicone, but the viscosity ratio was estimated as less than 1.5:1 and no attempt was made to measure it exactly. Plasticine in contrast has a strongly non-linear dependence of stress upon strain rate (McClay 1976). It sometimes exhibits strain-softening, leading to shear-band formation and failure. These properties render it suitable for making relatively resistant layers that are to boudinage.

Model construction

Models were constructed in layers within a special mould with overall dimensions of 40 × 10 × 5 cm. Individual layers (2–5 mm thick) were prepared by pressure moulding (silicone) or rolling (plasticine). The physical properties of the silicone are such that immediate bonding is ensured when layers are assembled. Initial deflections were introduced midway through the assembly process, by indenting the layer surface with a rigid object of known shape. Once assembled, the models were cooled to −30°C in a commercial freezer to facilitate handling and insertion in the deformation apparatus.

Model deformation

Models were deformed in a simple shear machine (Fig. 8) designed for attaining large shear strains ($\gamma < 30$). The sliding plates (Fig. 8) are of finite thickness (5 mm) and hence at high shear strains they cause some boundary perturbations. Friction against the lateral perspex walls was minimized using a liquid soap as lubricant. To assess the boundary conditions on the models, a test was conducted on a rheologically homogeneous silicone model with passive colour banding. Ideally such a model should undergo in the machine a homogeneous simple shear. In fact, friction at the lateral walls causes some departure from this behaviour. However, the external dimensions of the model are such that even with perfect adherence at the lateral walls, the resulting boundary disturbance decays rapidly with distance from the walls and is negligible at a distance of 1 cm (Fig. 9). It does not follow of course that boundary disturbances will decay rapidly if deformation is internally unstable. Liquid soap, however, greatly reduces the effects of friction.

Dissection of models

After deformation of the model, the entire shear machine was cooled to − 30°C before the model was extracted. It could then be handled and even cut without causing significant internal deformation. Serial sections were cut and photographed while cold. The three dimensional geometry of internal structures was reconstructed from the photographs using an isometric projection. The technique of total dissection has of course one major disadvantage: the model cannot be reassembled and used to study further stages of deformation. Instead the experiment must be repeated with a new model.

APPENDIX 2

STEADY-STATE SHEARING IN A NEWTONIAN HALF-SPACE BOUNDED BY A RIGID BED WITH PERIODIC ASPERITIES OF FINITE AMPLITUDE

We consider the slow two-dimensional deformation of a Newtonian fluid, where the velocity vector at each point has components v_ξ and v_η along orthogonal curvilinear coordinates, ξ, η (see Borg 1963, chapter 3, for a discussion of curvilinear coordinates). If there are no volume changes, the velocities can be expressed as

$$v_\xi = -h\frac{\partial U}{\partial \eta};\quad v_\eta = +h\frac{\partial U}{\partial \xi} \tag{1}$$

where $U(\xi, \eta)$ is a stream function (Jaeger 1969, p. 140) and h is a magnification factor for the curvilinear coordinates (Borg 1963). For a Newtonian fluid, it can be shown (Jaeger 1969, p. 140) that U satisfies the biharmonic equation,

$$\nabla^2(\nabla^2 U) = 0. \tag{2}$$

In Cartesian coordinates, general solutions to (2) can be written in terms of the complex argument $z = x + iy$ (Jaeger & Cook 1971, p. 231):

$$U = \tfrac{1}{2}\left|z\overline{\varphi(z)} + \bar{z}\varphi(z) + \psi(z) + \overline{\psi(z)}\right| \tag{3}$$

where φ and ψ are analytic functions of z and the bar denotes a complex conjugate. Techniques of conformal representation may be used to obtain solutions in terms of non-Cartesian coordinates (Mushkelishvili 1953). We consider the transformation

$$z = \zeta + A\exp w\zeta \tag{4}$$

where $\zeta = \xi + i\eta$ is a complex argument, A is a constant amplitude and w is a constant wavenumber. Equation (4) transforms the straight lines ξ = constant and η = constant into orthogonal curvilinear coordinates (Fig. 6). The magnification factor is given by (Borg 1963)

$$\frac{1}{h^2} = \left\{\frac{\partial x}{\partial \xi}\right\}^2 + \left\{\frac{\partial y}{\partial \eta}\right\}^2 = 1 + 2Aw\exp w\xi\cos w\eta + A^2w^2\exp 2w\xi. \tag{5}$$

If we choose the functions φ and ψ as follows:

$$\varphi = \frac{K}{4}(\zeta - A\exp w\zeta)\quad ;\psi = K - 4(\zeta^2 + 2A^2 w\zeta) \tag{6}$$

where K is a constant giving the intensity of the flow, then from (3);

$$U = K(\tfrac{1}{2}\xi^2 - \tfrac{1}{4}A^2\exp 2w\xi + \tfrac{1}{2}A^2 w\xi) \tag{7}$$

and from (1) the velocities are

$$v_\xi = 0;\ v_\eta = Kh\{\xi + \tfrac{1}{2}A^2 w(1 - \exp 2w\xi)\}. \tag{8}$$

The component v_η vanishes at the boundary $\xi = 0$ (indicating perfect adhesion) and becomes $K(\xi + \frac{1}{2}A^2w)$ at a large distance from it. Thus the solution represents shear flow over a bed with periodically spaced asperities of finite amplitude. A. Because $v_\xi = 0$, the η-coordinate lines are stream lines. For steady motion, they are also particle pathlines and the travel time, t, of a particle leaving the line $\eta = 0$ is:

$$\int_0^\eta \frac{d\eta}{v} = \left[K/\{\xi + \tfrac{1}{2}A^2w(1 - \exp 2w\xi)\}\right]\cdot\int_0^\eta \frac{d\eta}{h} \tag{9}$$

Using the value of h given in (5), we may integrate to obtain

$$t = \frac{2K(1 + Aw\exp w\xi)}{w\{\xi + \tfrac{1}{2}A^2w(1 - \exp 2w\xi)\}}\cdot E(k, \alpha) \tag{10}$$

where $E(k,\alpha)$ is a standard elliptic integral of the second kind, with arguments

$$k = \frac{2(Aw\exp w\xi)^{1/2}}{1 + Aw\exp w\xi};\ \alpha = \frac{w\eta}{2}. \tag{11}$$

Using (10) one can compute the new positions of particles after a finite time interval. The fold of Fig. 6(b) has been produced in this way.